Supplement of

Changing pattern of ice flow and mass balance for glaciers discharging into the Larsen A and B embayments, Antarctic Peninsula, 2011 to 2016

H. Rott et al.

Correspondence to: Helmut.Rott@enveo.at

Contents

Section S1 – Overview on glacier basins for retrieval of volume change and mass balance

The outlines of the glacier basins for retrieval of volume change and mass balance are displayed on a Landsat image (Figures S1 and S2). Table S1 contains a list of the basins with area extent in 2013 and 2016 and the GLIMS ID for the main glacier in each basin.

Section S2 – Data coverage by TanDEM-X interferometric SAR data

A map with area coverage of the TanDEM-X SAR image tracks used for DEM retrieval is shown (Fig. S3) and the specifications of the DEMs used for generating surface elevation change (SEC) products are listed (Table S2).

Section S3 – Estimation of uncertainty for surface elevation change and mass budget

Details are presented on the procedures and data base for estimating the uncertainty of the TanDEM-X maps of surface elevation change and on the mass balance obtained by DEM differencing and by the mass budget method.

Section S4 – TerraSAR-X image with ice mélange and sea ice in proglacial fjord

A TerraSAR-X image is shown in order to illustrate typical patterns of ice mélange and sea ice in proglacial fjords during years of persistent sea ice cover.

Section 1 – Overview on glacier basins for retrieval of volume change and mass balance

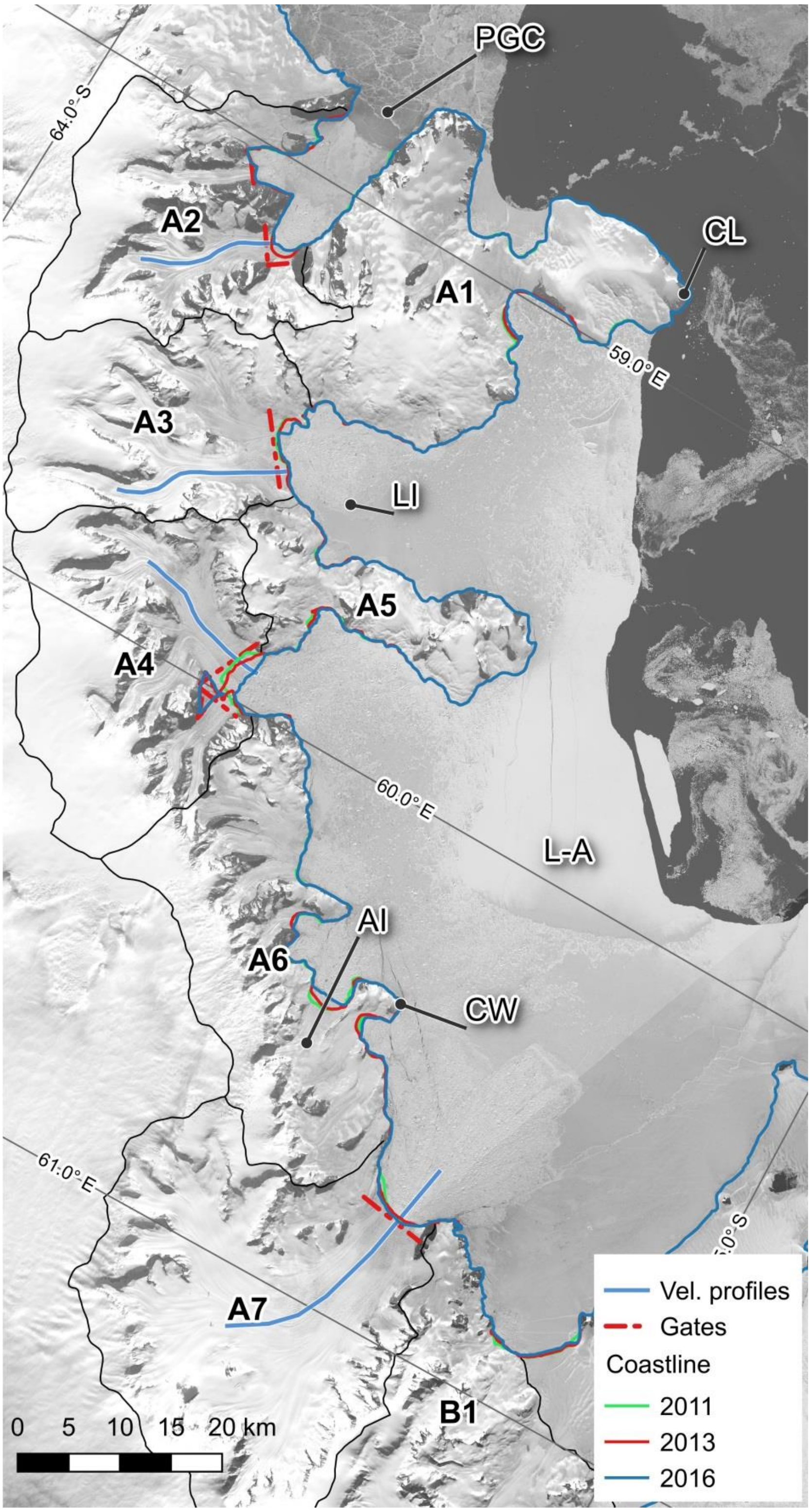

Figure S1. Outlines of glacier basins plotted on Landsat image of 2016-10-29. Coastlines from TanDEM-X images mid-2011, -2013, -2016. AI -Arrol Icefall, CW – Cape Worsley, CL- Cape Longing, L-A - Larsen A embayment, LI - Larsen Inlet, PGC – Prince Gustav Channel Red broken lines: gates for calving fluxes. Blue lines: Ice velocity profiles.

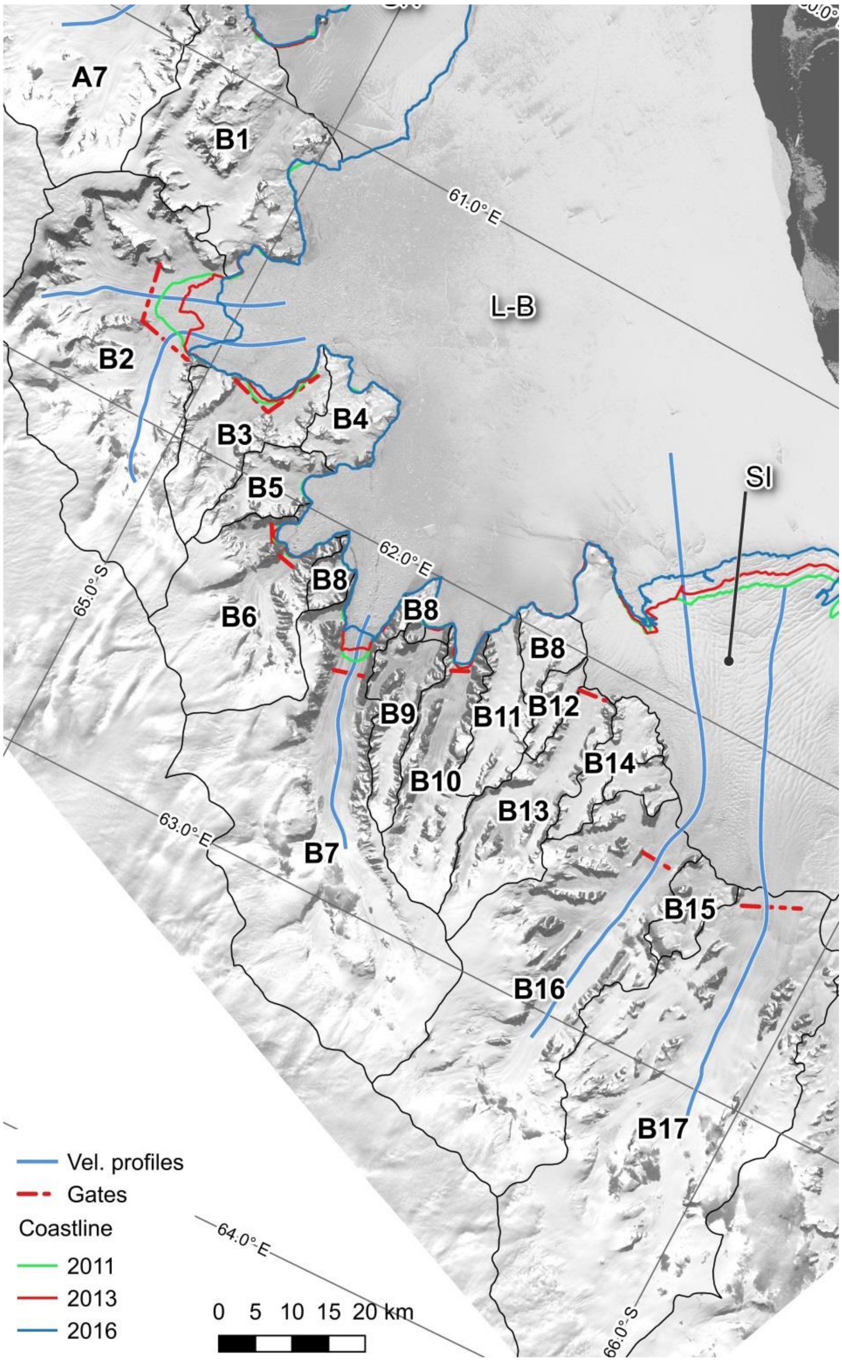

Figure S2. Outlines of glacier basins plotted on Landsat image of 2016-10-29. Coastlines from TanDEM-X images mid-2011, -2013, -2016. L-B - Larsen B embayment, SI – SCAR Inlet ice shelf. Red broken lines: gates for calving fluxes. Blue lines: Ice velocity profiles.

Table S1. Glacier catchments on northern Antarctic Peninsula (API) for retrieval of surface elevation change (SEC) and mass balance. Basin outlines inland are from the data set of Cook et al. (2014). The position of glacier fronts 2013 and 2016 are from geocoded TerraSAR-X images of June & July 2013 and July & August 2016.

Nr.	***Glacier Basin Name***	***Area [km^2]***		***GLIMS ID Nr. (main glaciers of basin)***
		2013	**2016**	
A1	Cape Longing Peninsula	667.30	668.91	G300465E64251S
A2	Sjørgen-Boydell, SB	525.47	527.55	G300700E64157S
A3	Albone, Pyke, Polaris,Eliason, APPE	511.29	513.58	G300465E64251S
A4	Dinsmoor, Bombardier-Edgeworth, DBE	646.50	653.93	G299838E64288S
A5	Sobral Peninsula	256.63	257.90	G300323E64397S
A6	Cape Worsley Coast	619.39	625.07	G299805E64456S
A7	Drygalski	998.54	998.32	G298872E64662
B1	Six glaciers west of Seal Nunataks	638.07	638.66	G298833E64908S
B2	Hektoria Green, HG	1167.49	1215.35	G298013E64919S
B3	Evans	266.92	272.32	G297915E65081S
B4	Evans Glacier Headland	117.66	117.66	G298295E65188S
B5	Punchbowl	119.94	119.88	AQ7LAB000009
B6	Jorum	460.33	461.41	G297567E65197S
B7	Crane	1322.57	1333.41	G297010E65410S
B8	3 small basins at Larsen B coast	142.64	142.64	G297840E65267S, G297936E65370S G297950E65543S
B9	Mapple	155.43	155.43	G297654E65415S
B10	Melville	291.47	292.91	G297326E65499S
B11	Pequod	150.35	150.58	G297685E65521S
B12	Rachel	51.80	51.80	G297822E65579S
B13	Starbuck	299.38	299.38	G297312E65606S
B14	Stubb	108.34	108.34	G297847E65684S
B15	2 small basins draining to SCAR Inlet ice shelf	136.78	136.78	G297762E65716S G297484E65849S
B16	Flask	1130.58	1130.58	G296666E65721S
B17	Leppard	1851.02	1851.02	G297153E65938S

Section 2 – Data coverage by TanDEM-X interferometric SAR data

Table S2. Raw DEMs processed as basis for generating SEC products. B6 and B9, respectively C4 and C7, include sequential sections of the same swath. Date refers to image acquisition. HoA is height of ambiguity. All images are descending equator crossing / right looking. Incidence angle refers to mid-swath. For spatial coverage see Fig. S.3.

Scene Label	Master / Slave	Date	HoA [m]	Rel. Orbit	Incidence. Angle
A	M	2013-10-02	-174.08	34	38.4
B6	M	2013-07-01	-60.64	125	45.6
B9	M	2013-07-01	-60.64	125	45.6
C4	M	2013-06-20	-56.73	125	40.6
C7	M	2013-06-20	-56.73	125	40.6
D	M	2013-06-09	-53.31	125	38.4
E	M	2013-05-18	-52.23	125	36.1
F	M	2013-07-29	-68.93	49	40.6
A	S	2016-07-10	-27.65	34	38.4
B6	S	2016-08-07	-26.64	125	45.6
B9	S	2016-08-07	-26.64	125	45.6
C4	S	2016-07-27	-29.11	125	40.6
C7	S	2016-07-27	-29.11	125	40.6
D	S	2016-07-16	-27.55	125	38.4
E	S	2016-08-18	-20.62	125	36.1
F	S	2016-07-22	-29.69	49	40.6
11A	S	2011-05-06	-50.59	34	37.3
11B	S	2011-06-30	51.80	34	36.1
11C	S	2011-06-25	57.62	125	41.0

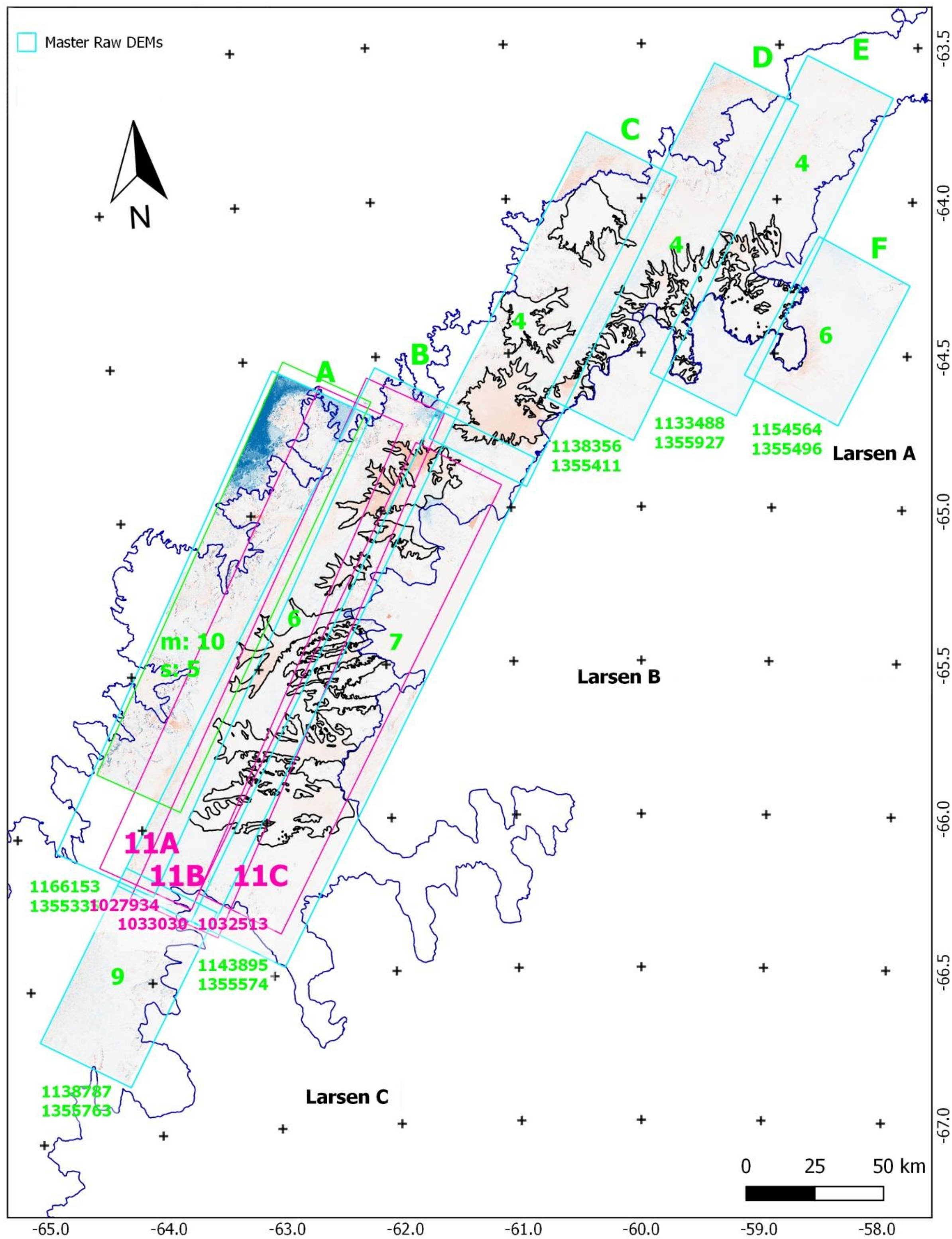

Figure S3. Geographic coverage of TanDEM-X tracks for generating DEMs and maps of surface elevation change. Red: tracks for 2011 DEMs. Green: tracks for 2013 to 2016 DEMs. Data specifications in Table S2.

Section 3 – Estimation of uncertainty for surface elevation change and mass budget

3.1 DEM differencing

For estimating the uncertainty of the TanDEM-X (TDM) elevation change product we compare TDM SEC data over the time span 2011 to 2016 with surface elevation rate of change data (dh/dt, product code IDHDT4) derived from Airborne Topographic Mapper (ATM) swathes, acquired during NASA IceBridge campaigns on 2011-11-14 and 2016-11-10 (Studinger, 2014, updated 2017). Each IDHDT4 data record corresponds to an area where two ATM lidar swathes have co-located measurements. The IDHDT4 data are provided as discrete points representing 250 m x 250 m surface area and are posted at about 80 m along-track spacing. We compare mean values of cells comprising 7 x 7 TDM dh/dt pixels (of about 12 m x 12 m pixel size) with the corresponding IDHDT4 points along flowlines of six glaciers (Table S3). The ATM profiles extend from the ice front (on Leppard Glacier from a position several km up-glacier) up to different altitudes. On Drygalski Glacier and Crane Glacier we start the comparison several km inland of the front, because the lower sections of the terminus are very crevassed and the ice front positions differed on the dates of the ATM and TDM DEM acquisitions. A small percentage of the ATM dh/dt data shows high RMS (in crevasse zones and on steep slopes); these points are not used for the comparison.

Table S3. Mean rates of elevation change (dh/dt) 2011 to 2016 measured by ATM and TanDEM-X (TDM) for longitudinal profiles on Larsen outlet glaciers. $\Delta\langle dh/dt\rangle$ - difference of mean dh/dt (ATM – TDM.) RMSD – root mean square difference.

Glacier	dh/dt [m a^{-1}] ATM 2011-16	dh/dt [m a^{-1}] TDM 2011-16	$\Delta\langle dh/dt\rangle$ [m a^{-1}]	RMSD [m a^{-1}]	Nr. ATM samples
Crane	-2.460	-2.472	+0.012	0.219	238
Flask	-1.346	-1.272	-0.074	0.149	172
Leppard	-1.092	-0.896	-0.196	0.218	205
Melville	-1.362	-1.299	-0.063	0.232	165
Starbuck	-0.459	-0.309	-0.156	0.172	41
Drygalski	-4.707	-4.663	-0.044	0.350	92

For the error analysis we assume that the differences result from uncertainties in both data sets. We assume for RMSD = 0.28 m a^{-1} (as representative value), resulting in RMSE = 0.20 m a^{-1} at the scale of individual cells for the each of the two data sets. This number is valid for a dh/dt time span of 1 year, derived from Δh measurements over a time span of 5 years.

Measurements for the shorter periods (2 years, 3 years) are scaled accordingly. In addition, we include uncertainty estimates for a possible bias, with bulk values for the mapped area below the escarpment, the unsurveyed slopes, and the ice plateau.

The following formulation is applied for estimating the uncertainty of volume change, $E_{\Delta V}$ [$m^3\ a^{-1}$], for a glacier basin covering an area A_B:

$$E_{\Delta V} = A_B \sqrt{f_m \frac{S_e^2}{n} + f_m E_m^2 + f_p E_p^2} \qquad \text{Eq. S1}$$

The following values are used to obtain annual rates of volume change for the Larsen glacier basins, based on Δh measurements over time spans of 2 years (2011-2013) and 3 years (2013-2016):

- S_e, random error for the TDM dh/dt map: S_e = 0.58 m a^{-1} (Δh 2 yr); S_e = 0.39 m a^{-1} (Δh 3 yr)
- E_m, possible bias for TDM dh/dt maps below the escarpment: E_m = 0.075 m a^{-1} (Δh 2 yr); E_m = 0.05 m a^{-1} (Δh 3 yr)
- E_p, possible bias for dh/dt on ice plateau and on unsurveyed slopes: E_p = 0.15 m a^{-1} (Δh 2 yr); E_p = 0.10 m a^{-1} (Δh 3 yr)

For the first term under the square-root an estimate for the number of statistically independent samples (n) is needed, accounting for spatial correlation. We assume a distance of 500 m for spatial decorrelation. The second term accounts for a possible bias of the TDM dh/dt maps below the escarpment. The factors f_m and f_p account for the extent of the respective area relative to the total basin area. The bias estimates for the ice plateau and the unsurveyed slopes are also deduced from the comparison of ATM and TDM dh/dt data. They are based on the first two terms under the square root of Eq. S1, applying f_m = 1.0, n = 80, and increasing the resulting value by 50 % to allow for an additional margin.

For converting volume change to mass change we assume a mean density ρ = 900 kg m^{-3}. This value is commonly used for geodetic mass balance studies in case the mean density of the snow/ice column does not change. From the similarity of the radar backscatter coefficients in the 2011 and 2016 TanDEM-X images we can exclude significant changes in the structure and density of the snow/firn column. The good agreement between the IceBridge lidar based dh/dt values and the TanDEM-X based dh/dt values indicates also stability of the structure and density of the snow/ice medium. Changes of density and structure would cause a vertical shift of the radar scattering phase centre within the volume, resulting in a relative shift of the surface in the SAR DEM data versus the surface in the optical data (Dall, 2007). The stability of radar backscatter and the good agreement of optical and radar dh/dt indicate that the possible error due to density changes in the vertical column is negligible compared to the uncertainty in dh/dt. Scambos et al. (2014) use also a mean density of 900 kg m^{-3} for converting volume change into mass for their mass balance analysis of glaciers on the northern Antarctic Peninsula over the period 2001 to 2010, so that these mass changes can be directly compared with our estimates.

For estimating the uncertainty of sub-regions (Larsen A, Larsen B embayment, SCAR Inlet) we assume that the errors for glaciers covered by a single TDM track are correlated (the errors are added) and the errors of different tracks are uncorrelated.

3.2 Mass budget method

The uncertainty estimate for mass balance at basin scale, derived by means of the mass budget method, accounts for uncertainties of surface mass balance (SMB) and for uncertainties in flow velocity and ice thickness at the flux gates. The SMB is based on output of the regional climate model RACMO Version 2.3p2 (van Wessem et al., 2016; 2017). For the uncertainty of surface mass balance at basin scale we assume ± 15 % uncertainty for the average SMB. This value is based on an evaluation of the RACMO SMB output on the Antarctic Peninsula, showing good agreement with the balance flux of Larsen B glaciers in pre-collapse state (van Wessem et al., 2016).

The velocities used for computing calving fluxes are exclusively derived from TerraSAR-X and TanDEM-X repeat pass data. The uncertainty in the magnitude of the TerraSAR-X derived surface motion product over Larsen B glaciers at 50 m grid size is estimated at ±0.05 m d^{-1} (details in Wuite et al., 2015). Besides, we performed a direct comparison between GPS velocity measurements at stakes made by British Antarctic Survey (BAS) over annual intervals 2009/2010 and 2011/2012 on Flask Glacier and 2011/2012 on Starbuck Glacier. (GPS data kindly made available by BAS for the ESA project GlacAPI: https://glacapi.enveo.at/). Although the TerraSAR-X measurements cover shorter intervals, the agreement is very good: The differences between GPS and TerraSAR-X velocities at the individual stakes are within ±0.01 m d^{-1}; the stake velocities ranging from 0.71 to 0.95 m d^{-1} on Flask Glacier and 0.13 to 0.18 m d^{-1} on Starbuck Glacier. This confirms that an uncertainty estimate of ±0.05 m d^{-1} at 50 m grid size is a rather conservative estimate for the TerraSAR-X/ TanDEM-X based velocity product. For computing calving fluxes we assume ± 5 % uncertainty in velocity across the gate. For uncertainty estimates of mass fluxes we assume ± 10 % error for the cross section area of glaciers with GPR data across or close to the gates and

± 15 % for glaciers where the ice thickness is deduced from frontal height above flotation measured by TanDEM-X (relative 90 % point-to-point height error <2 m; Rizzoli et al., 2012).

Section 4 – TerraSAR-X image with ice mélange and sea ice in proglacial fjord

Figure 4 shows typical patterns of ice mélange (a mixture of icebergs and bergy bits, held together by sea ice) in the fjord in front of Crane, Jorum and Punchbowl glaciers, and sea ice with a larger iceberg in the wider section of the bay.

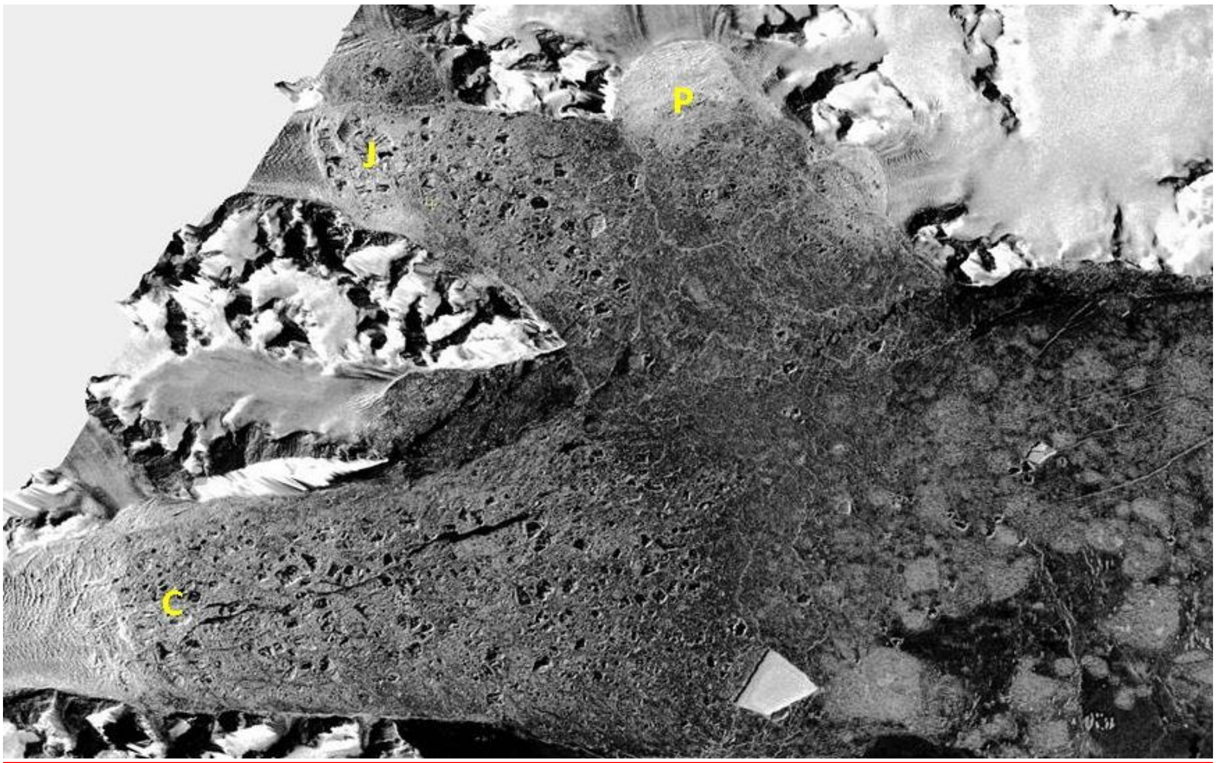

Figure S4. Section of TerraSAR-X amplitude image, acquired on 27 July 2016, with calving fronts of Crane (C), Jorum (J) and Punchbowl (P) glaciers and the proglacial fjord covered by ice mélange and sea ice.

References

Dall, J.: InSAR elevation bias caused by penetration into uniform volumes. IEEE Trans. Geosc. Remote Sensing, 45(7), 2319–2324, 2007.

Rizzoli, P., Bräutigam, B., Kraus, T., Martone, M., and Krieger, G.: Relative height error analysis of TanDEM-X elevation data, ISPRS J. Photogrammet. Remote Sens., 73, 30–38, 2012.

Scambos, T. A., Berthier, E., Haran, T., Shuman, C. A., Cook, A. J., Ligtenberg, S. R. M., and Bohlander, J.: Detailed ice loss pattern in the northern Antarctic Peninsula: widespread decline driven by ice front retreats, The Cryosphere, 8, 2135-2145, doi:10.5194/tc-8-2135-2014, 2014.

Studinger, M. S: IceBridge ATM L4 Surface Elevation Rate of Change, Version 1, Subset M699, S10, Boulder, Colorado USA. NASA National Snow and Ice Data Center Distributed Active Archive Center, doi: http://dx.doi.org/10.5067/BCW6CI3TXOCY, [Accessed 25 July 2017], 2014, updated 2017.

van Wessem, J. M., Ligtenberg, S. R. M., Reijmer, C. H., van de Berg, W. J., van den Broeke, M. R., Barrand, N. E., Thomas, E. R., Turner, J., Wuite, J., Scambos, T. A., and van Meijgaard, E.: The modelled surface mass balance of the Antarctic Peninsula at 5.5 km horizontal resolution, The Cryosphere, 10, 271-285, 2016.

van Wessem, J. M., van de Berg, W. J., Noël, B. P. Y., van Meijgaard, E., Birnbaum, G., Jakobs, C. L., Krüger, K., Lenaerts, J. T. M., Lhermitte, S., Ligtenberg, S. R. M., Medley, B., Reijmer, C. H., van Tricht, K., Trusel, L. D., van Ulft, L. H., Wouters, B., Wuite, J., and van den Broeke, M. R.: Modelling the climate and surface mass balance of polar ice sheets using RACMO2, part 2: Antarctica (1979–2016), The Cryosphere Discuss., https://doi.org/10.5194/tc-2017-202, in review, 2017.